JSR Publications

Available Online

J. Sci. Res. **17** (3), 951-965 (2025)

JOURNAL OF SCIENTIFIC RESEARCH

www.banglajol.info/index.php/JSR

A Combined Theoretical and Experimental Approach to a Tyrosine Derivative with Anticancer Activity

D. Ganasaraswathy, P. Vijaya*

Department of Chemistry, Rani Anna Government College for Women, Tirunelveli-627008, Tamil Nadu, India (Affiliated to Manonmaniam Sundaranar University, Abishekapatti, Tirunelveli-627012, Tamilnadu, India)

Received 14 February 2025, accepted in final revised form 16 June 2025

Abstract

4-((E)-2-(4-isopropylbenzylideneamino)ethyl)phenol (4TC) has been synthesized and characterized using spectral studies including UV-Visible and FT-IR. The anti-cancer activity of 4TC was evaluated using the MTT assay against two cancer cell lines: MDA MB 231 (human breast cancer cell line) and A549 (human lung cancer cell line). The optimized structure of 4TC is computationally constructed and theoretically studied using Gaussian 03 with the Density Functional Theory (DFT) method. This utilized the B3LYP functional with the 6-31G(d,p) basis set. Vibrational frequencies were analyzed using potential energy distribution (PED%) calculations through the vibrational energy distribution analysis (VEDA 4) program. Nonlinear optical (NLO) properties were examined based on calculated values of dipole moment (μ), polarizability (α), and first hyperpolarizability (β_tot). The polar sites of the molecules were identified using molecular electrostatic potential (MEP) surfaces, while orbital overlap was determined through the HOMO-LUMO analysis. Additionally, the electron affinity, electronegativity, chemical potential, hardness, and softness of the compounds were characterized via frontier molecular orbital (FMO) studies. In the in-silico evaluation, physicochemical parameters and drug-likeness were predicted using Swiss-ADME and pre-ADME web tools. Finally, in silico antibacterial and antifungal activity percentages were assessed using the PASS (Prediction of Activity Spectra for Substances) online tool.

Keywords: DFT; UV; FT-IR; Anti-cancer; Hyperpolarizability; MEP; FMO; ADMET.

doi: https://dx.doi.org/10.3329/jsr.v17i3.79829 J. Sci. Res. **17** (3), 951-965 (2025)

1. Introduction

Density Functional Theory (DFT) has emerged as a powerful tool for studying the structural, electronic, and reactivity properties of various organic compounds, including tyrosine derivatives [1]. It provides valuable insights into the molecular characteristics and behavior of these compounds, enabling researchers to predict and understand their properties at the atomic and electronic levels. DFT methods offer a robust approach for

* *Corresponding author:* ganasaraswathyresearch@gmail.com

investigating tyrosine derivatives and other organic compounds. The ability of DFT to provide accurate electronic structure calculations and elucidate reaction mechanisms [2] makes it an invaluable tool for researchers seeking to understand and predict the properties of these molecules. The 6-31G(d,p) basis set was employed in this study as a compromise between computational efficiency and accuracy. While it is a relatively modest basis set, it has been shown to provide qualitatively reliable results for systems of similar size and complexity. Additionally, the inclusion of polarization functions (d,p) helps improve the description of electron distribution and molecular geometries. Nonetheless, we acknowledge that larger basis sets may yield more quantitatively accurate results, and future work could explore these to further validate the current finding**s.** The MTT (3-(4,5-dimethylthiazol-2-yl)-2,5-diphenyltetrazolium bromide) assay is widely used to measure cell proliferation and screen for anticancer drugs [3]. It is based on the reduction of MTT by actively growing cells to produce a blue formazan product. Several studies have utilized this assay to evaluate the cytotoxic effects of different compounds on cancer cell lines. ADME prediction for tyrosine derivatives likely involves a combination of computational methods and experimental approaches. Quantitative proteomics analysis of drug-metabolizing enzymes and transporter**s** can provide key physiological information to assist in translating in vitro and preclinical data to humans [4]. Integration of this data into physiologically based pharmacokinetic modelling is proving critical for safe, effective, timely, and cost-effective drug development. As research in this field progresses, it is expected that more accurate and comprehensive ADME prediction methods for tyrosine derivatives will be developed. By using the PASS-online tool (Prediction of Activity Spectra for Substances), the antibacterial and antifungal activities of 4TC are predicted [5].

2. Experimental Details

The solvents and chemicals were obtained from commercial sources like Sigma Aldrich. The FT-IR spectrum of the tyrosine derivative is recorded by the Perkin Elmer FTIR spectrometer in the range of 4000 cm^{-1} to 400 cm^{-1} using KBr pellets. The UV-Vis absorption spectrum of 4TC is obtained by dissolving the compound in ethanol, which is examined in the range of 190 nm to 1100 nm using a double-beam microprocessor UV-VIS touch screen spectrophotometer with software (Model No. Li-2900). The cell lines that were used in the MTT assay for anti-cancer analysis were obtained from the National Centre for Cell Sciences (NCCS), Pune, India. All the experiments concerning the cytotoxicity evaluation were performed and analyzed by Athmic Biotech Solutions Pvt. Ltd., Thiruvananthapuram, India.

3. Computational Techniques

All the computational studies are carried out at the density functional theory level using Gaussian 03W software. DFT calculations lead to good accuracy and are less time-consuming. The calculations are carried out with Becke's three-parameter exchange functional with the LYP correction (B3LYP), and the basis set 6-31G (d,p) is used in

appropriate calculations. The computational work has begun with the conformational analysis of the compounds. IR vibrational frequencies of the molecule are interpreted by means of potential energy distribution (PED%) calculation using the Vibrational Energy Distribution Analysis (VEDA) program. The UV-Vis absorption studies were carried out at the TDSCF/6-31G (d,p) basis level. The normal modes assignment of the theoretical IR frequencies is envisioned and validated with the help of the Gauss View 5.0 visualization program. The polarizability calculation was done by the DFT method with a route section (polar = enonly). The dipole moment (μ), the mean polarizability (α), and the first hyperpolarizability (β_{tot}) are directly related to the nonlinear optical efficiency of structures. The molecular electrostatic potential (MEP) surface has been plotted for the molecule and its cationic and anionic forms. Highest occupied molecular orbital (HOMO) and lowest unoccupied molecular orbital (LUMO) pictures are drawn, and the HOMO-LUMO energy gap is calculated.

4. Result and Discussion

4.1. *Geometry optimization*

The compound 4TC is theoretically constructed and optimized with the basis set DFT/B3LYP-6-31G (d,p). The compound 4TC has 41 atoms and 144 electrons with the C1 point group. Numbering for the optimized structures for 4TC is shown in Figure 1. The heat of formation value of the compound 4TC is -828.570944 kcal/mol [6-9]. The geometric properties, including bond length, bond angle and torsion angle, are tabulated in Table 1. The bond length of C_{10}=N_{11} in 4TC is 1.27 Å, and the bond length of the electron-donating group (-$CH(CH_3)_2$) bonded to the benzene ring is 1.52 Å.

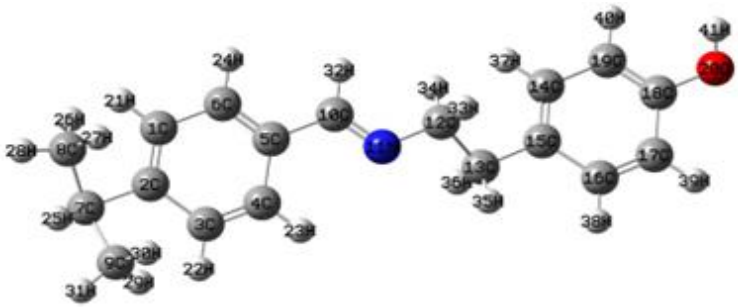

Fig. 1. Optimized structure of 4TC.

Table 1. Selected geometric parameters of 4TC are computed by the DFT/B3LYP-6-31 G (d,p) basis set.

Bond	Bond length(Å)	Bond	Bond length(Å)	Bonds	Bond angle(°)
C1-C2	1.39	C7-C9	1.54	C12-C13-C15	112.6
C2-C3	1.40	C5-C10	1.47	N11-C12-C13	110.5
C3-C4	1.38	C10-N11	1.27	N11-C10-C5	123.1
C4-C5	1.40	N11-C12	1.45	C2-C7-C8	111.8
C5-C6	1.40	C12-C13	1.54	C2-C7-C9	111.7

C6-C1	1.39	C13-C15	1.51	Bonds	Torsinal Angle (^{0})
C2-C7	1.52	C15-C16	1.40	C15-C13-C12-N11	-175.6
C7-C8	1.50	C16-C17	1.39	C5-C10-N11-C12	179.4
C17-C18	1.39	C14-C15	1.39	-	-
C18-C19	1.39	C18-O20	1.36	-	-
C19-C14	1.39	-	-	-	-

4.2. *FT-IR analysis*

The theoretical FT-IR vibrational frequencies of the compound 4TC have been constructed using the DFT method with a 6-31G (d,p) basis set shown in Figure 2. It consists of 41 atoms and hence correspondingly has 117 normal modes of vibration, which include 40 stretching, 39 bending, and 38 torsional modes of vibration. The molecule 4TC belongs to C1 symmetry. All the modes are IR active modes [10]. The calculated IR frequencies are scaled by a factor of 0.9614. The significant experimental, unscaled, and scaled computed IR frequencies are given in Table 2. In addition, theoretical IR vibrational spectra are interpreted by means of potential energy distribution (PED%) calculation using the vibrational energy distribution analysis (VEDA) [11] program. The normal mode assignment of the theoretical IR frequencies is visualized with the help of the GaussView 5.0 program. None of the predicted vibrational IR frequencies have any imaginary frequency, implying that the optimized geometry is located at the local minimum point on the potential energy state.

The aromatic C-H stretching frequencies appear in the range of 3100–3000 cm^{-1} [12]. The aromatic ring C-C stretching vibrations occur in the region 1650-1400 cm^{-1} [13]. In this study, the experimental IR frequency of the aromatic stretching frequency of C1-H21 and C6-H24 appears at 3045 cm^{-1} and 3021 cm^{-1}, which overlaps with modes 114 and 109, which corresponds to the theoretical aromatic C-H stretching vibration. The higher PED% of the C-H vibration in this mode with a scaled frequency of 3062 cm^{-1} and 3038 cm^{-1} predicts the purity of this aromatic C-H stretching vibration in this zone. The aromatic C-C stretching vibrations are found in the mode numbers 94, 91 and 83 and scaled frequencies ranging from 1602 to 1423 cm^{-1}, with the experimental IR frequency at 1609 cm^{-1}, 1514 cm^{-1} and 1419 cm^{-1}. The aromatic C-C-H bending vibrations are generally observed in the region 1300-1000 cm^{-1} [14,15]. The bands observed at 1303 cm^{-1}, 1158 cm^{-1}, 1137 cm^{-1}, 1102 cm^{-1} and 1014 cm^{-1} in the experimental IR spectra of the title compound are well explained by mode Nos. 76, 64, 62, 59 and 57 in the theoretical IR vibrational scaled frequencies at 1323 cm^{-1}, 1157 cm^{-1}, 1152 cm^{-1}, 1092 cm^{-1} and 1036 cm^{-1}, respectively. The aliphatic carbon stretching vibrations were observed in the range 2900 cm^{-1} to 3000 cm^{-1} [16,17]. The experimental value observed in the range of 2969 cm^{-1}, 2938 cm^{-1} and 2926 cm^{-1} in the experimental IR spectra is assigned to the vibration of H33-C12-H34, which is found in mode No. 104, 103, 101 and 100 in the corresponding theoretical IR vibrational study of 4TC with a scaled frequency between 2976 and 2923 cm^{-1} and is in accordance with the experimental value observed in the respective experimental IR spectra of 4TC. The C=N imine group vibration occurs at 1728 cm^{-1}, which is theoretically in accordance with the stretching frequency of 2868 cm^{-1} at mode 96 [18,19]. The aromatic

hydroxy group (OH) group is given by the vibrational frequency 3625 cm^{-1} with the theoretical vibrations of 3675 cm^{-1} at the mode no. 117 [20,21].

Table 2. Significant experimental and theoretical vibrational frequencies of 4TC.

Mode	Theoretical frequencies (cm^{-1}) DFT/B3LYP/6-31G(d,p)		Observed frequencies (cm^{-1})	Vibrational assignment PED ≥10 %
	Unscaled frequencies	Scaled frequency scaling factor = 0.9614		
117	3823	3675	3625	ν O20-H41 (100 %)
114	3185	3062	3045	ν C1-H21 (57 %) + ν C6-H24 (40 %)
109	3160	3038	3021	ν C14-H37 (20 %) + ν C19-H40 (79 %)
108	3121	3001	2960	ν C8-H26 (16 %) + ν C8-H27 (47 %) + ν C9-H30 (22 %)
107	3120	3000		ν C8-H27(22 %) + ν C9-H30 (51 %) + ν C9-H31 (10 %)
106	3114	2994		ν C8-H26 (26 %) + ν C8-H28 (37 %) + ν C9-H29(15 %) + ν C9-H31(17 %)
104	3096	2976	2969	ν C13-H35 (55 %) + ν C13-H36 (40 %)
103	3052	2934	2938	ν C13-H35 (35 %) + ν C13-H36 (26 %)
101	3044	2927	2926	ν C8-H26 (22 %) + ν C8-H27 (19 %) + ν C8-H28(25 %) + ν C9-H29(12 %) + ν C9-H31(12 %)
100	3040	2923		ν C8-H26 (12 %) + ν C8-H28 (13 %) + ν C8-H29(24 %) + ν C9-H30(17 %) + ν C9-H31(25 %)
98	2980	2865	2693	ν C10-H32 (97 %)
97	2963	2849	2650	ν C12-H34 (90 %)
96	1731	1664	1728	ν N11-C10 (79 %)
95	1975	1899	1899	ν C14-C19 (11 %) + ν C16-C17 (27 %) + ν C15-C14 (11 %) + ν C18-C17 (10 %)
94	1666	1602	1609	ν C3-C4 (30 %) + ν C6-C5 (12 %)
91	1562	1502	1514	ν C15-C14 (11 %) + β H37-C14-C19 (14 %) + β H38-C16-C17(14 %) + β H40-C19-C18(15 %)
83	1480	1423	1419	ν C14-C19 (10 %) + ν C16-C17 (13 %) + β H41-O20-C18 (10 %) + β H39-C17-C18(13 %)
77	1384	1331	1330	β H32-C10-N11 (10 %) + τ H33-C12-N11-C10 (19 %) + τ H34-C12-N11-C10 (22 %) + τ H35-C13-C15-C14 (10 %)
76	1376	1323	1303	ν C14-C19 (18 %) + ν C16-C17 (15 %) + ν C15-C14 (12 %) + ν C18-C17 (11 %) + β H41-O20-C18 (19 %) + β H38-C16-C17(13 %)
70	1306	1256	1242	ν O20-C18 (48 %)
64	1203	1157	1158	β H21-C1-C6 (16 %) + β H23-C4-C5 (14 %) + β H24-C6-C5 (20 %)
62	1198	1152	1137	ν C18-C17 (17 %) + β H41-O20-C18 (46 %) + β H39-C17-C18(12 %)
59	1136	1092	1102	ν C16-C17 (10 %) + β H37-C14-C19 (12 %) + β H38-C16-C17(15 %) + β H39-C17-C18(13 %)
57	1078	1036	1014	τ H26-C8-C7-C9 (12 %) + τ H29-C9-C7-C8 (12 %)

39	844	811	821	$\tau_{H38\text{-}C16\text{-}C17\text{-}C18}$ (27 %) + $\tau_{H39\text{-}C17\text{-}C18\text{-}C19}$ (34 %) + $\gamma_{O20\text{-}C17\text{-}C19\text{-}C18}$ (10 %)
18	347	334		$\tau_{418\text{-}O20\text{-}C18\text{-}C17}$ (94 %)

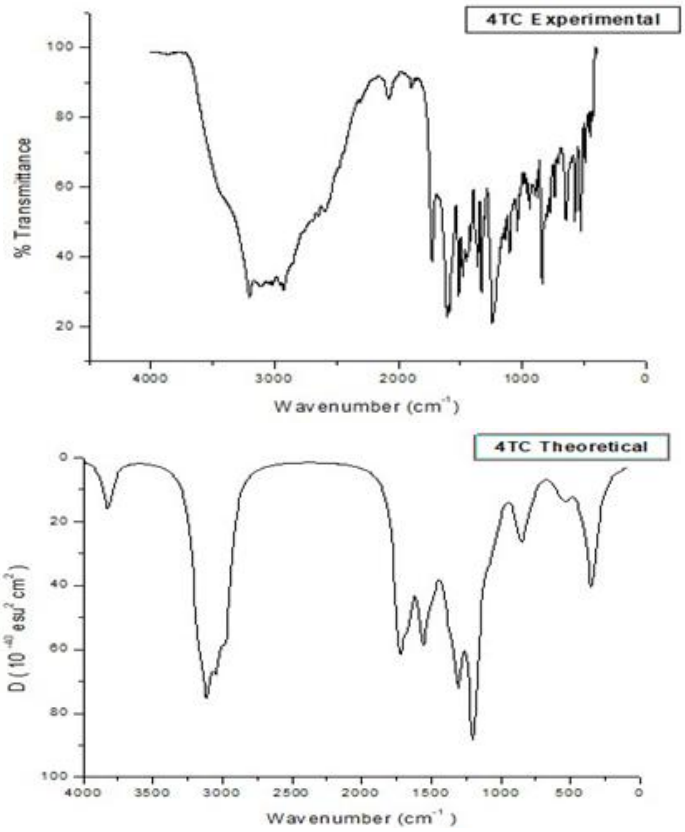

Fig. 2. Experimental and theoretical FT-IR spectra of 4TC.

4.3. *UV-Vis spectrum analysis*

The UV absorption spectrum of the title compound 4TC in ethanol was recorded within the 190-1100 nm range and represented in Fig. 3. It is observed that the recorded spectrum was maximum at 303 nm and minimum at 380 nm. The intense observed band in the spectra of 4TC can be assigned to the π-π* transition due to the presence of a C=N double bond conjugated with an aromatic ring. In order to support our experimental observations, DFT calculations on electronic absorption spectra were performed based on the TDSCF/6-31G(d,p) level-optimized structure [22]. The DFT method predicted the maximum absorption peak at 256 nm with strong oscillator strength, while this peak was recorded at 295 nm in ethanol. Solvent makes the chemical environment of a molecule in the simulation very complex. All the observed transitions are π-π* ones.

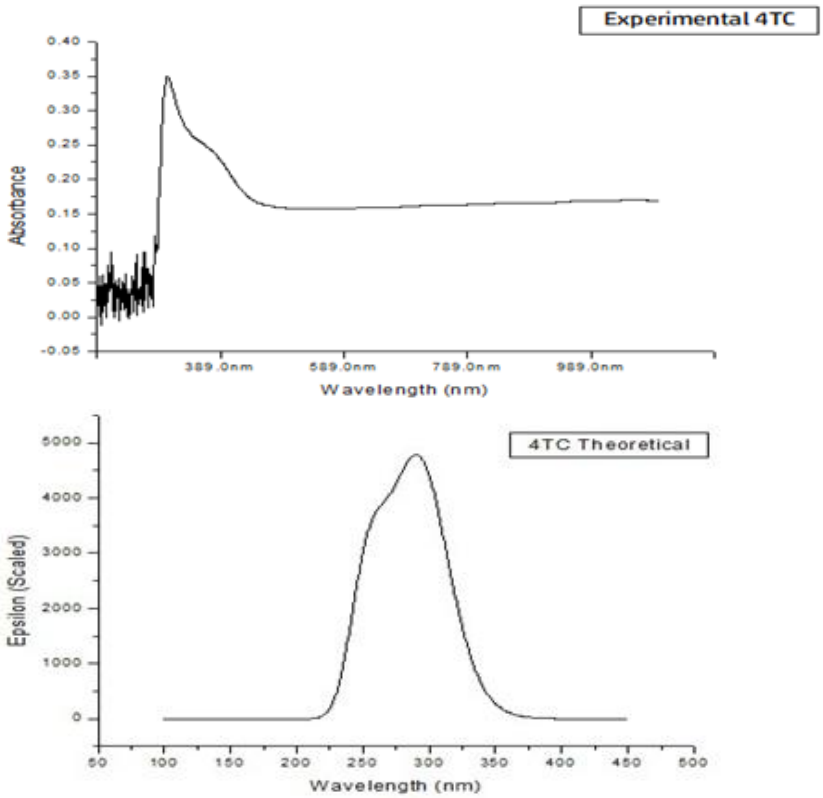

Fig. 3. Experimental and theoretical UV-Vis spectrum of 4TC.

4.4. *Hyperpolarizability*

In the present study, dipole moment (μ), polarizability (α_0), first hyper polarizability (β_{tot}) values are calculated using the finite field method, and the results are tabulated in Table 3 along with corresponding components [23-25]. Among dipole moment components, μ_y has the highest value for the 4TC molecule. The calculated polarizability also has non-zero values which are ascendant by the diagonal components. The delocalization of charges in a particular direction is indicated by the larger values of polarizability and first hyper polarizability. In 4TC, the first hyper polarizability is dominated by the β_{yyy} value. Table 3 reports the cartesian components of the dipole moment, polarizability, and hyperpolarizability tensors as computed in the molecular coordinate system used in the calculations. While these components are coordinate-dependent and do not have standalone physical significance, they are presented here to provide detailed insight into the tensor properties. For physically meaningful comparisons, the scalar (coordinate-invariant) quantities such as the total dipole moment (μ), polarizability (⟨α⟩), and the total first hyperpolarizability (β_tot) are also provided. The first hyperpolarizability (β) of 4TC is

approximately 50 % higher than that of urea, indicating its potential as a promising material with significant nonlinear optical (NLO) properties [26].

Table 3. The electric dipole moment μ(D), polarizability (α) (x 10^{-24} esu) and the first hyperpolarizability β_{tot} (x 10^{-33} esu) of 4TC by DFT method.

Parameter	Value	Parameter	Value
μ_x	0.35	β_{xxx}	18.44
μ_y	0.86	β_{xxy}	105.85
μ_z	0.14	β_{xyy}	22.01
μ	0.94	β_{yyy}	43.11
α_{xx}	345.90	β_{xxz}	73.27
α_{xy}	-1.63	β_{xyz}	22.31
α_{yy}	182.47	β_{yyz}	3.60
α_{xz}	17.54	β_{xzz}	4.82
α_{yz}	4.17	β_{yzz}	14.39
α_{zz}	111.92	β_{zzz}	5.25
(α)	213.43	β_{tot}	182.99

4.5. *MEP surface analysis*

The MEP is a three-dimensional representation of the electrostatic potential around a molecule. It combines the electron density with the Coulombic potential from the nuclear charges, giving a visual sense of the charge distribution in space [27-28]. It helps to identify regions of high reactivity, such as areas with high electron density. The red region represents negative potential, is nucleophilic in nature and is available for electrophilic attack. The blue region represents positive potential, electrophilic in nature and readily available for nucleophile attack. The green region is neutral. In compound 4TC, N_{11} and O_{20} are electrophilic attack sites having electron-rich centres. H_{41} is a nucleophilic attack site having electron-deficient centres. MEP surface is plotted for the compounds 4TC represented in Fig. 4.

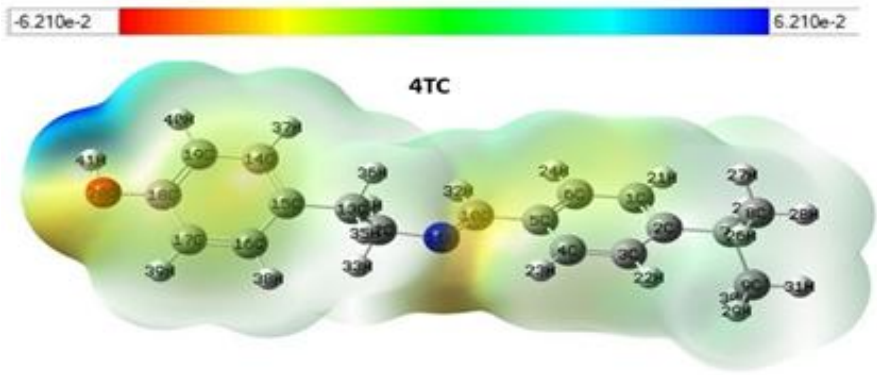

Fig 4. MEP surface of 4TC.

4.6. *FMO analysis*

The highest occupied molecular orbital (HOMO) reflects the ability of the molecule to donate electrons, which is related to the ionization potential, and the lowest unoccupied molecular orbital (LUMO) indicates the molecule's ability to accept electrons, which is related to electron affinity [29,30]. The energy difference between the HOMO and LUMO of the system is significant because it provides insights into the electronic properties of the molecule. It provides a qualitative idea about the molecule's reactivity, stability and optical properties. The HOMO-LUMO pictures of the compounds 4TC are shown in Fig. 5. In the compound 4TC, the atoms involved in HOMO are O20 and aromatic carbons from C14-C19 and the aliphatic carbons C13 and C12 with the atoms C5, C2, H36 and H35. The imine group N11 and C10 are involved in both HOMO and LUMO. Likewise, in LUMO, the aromatic atoms C1-C6 and the aliphatic carbon C9 are included. The HOMO-LUMO energy gap, chemical potential, hardness and softness, electronegativity and global philicity values of the compounds 4TC are represented in Table 4. The following formulas can be used to calculate the electronegativity (χ), chemical hardness (η) [31], softness (S), chemical potential (μ) [32], and globalphilicity (ω) [33]:

$$\eta = \frac{1}{2}[E_L - E_H] \quad (1)$$

$$S = \frac{1}{\eta} \quad (2)$$

$$\mu = \frac{(E_H + E_L)}{2} \quad (3)$$

$$\chi = \frac{-(E_H + E_L)}{2} \quad (4)$$

$$\omega = \frac{\mu^2}{2\eta} \quad (5)$$

The HOMO energy of 4TC is -5.779 eV, which indicates the ionization potential or the energy required to remove an electron from the molecule. The LUMO energy is -1.0533 eV, representing the electron affinity or the ability of the molecule to accept an electron. The bandgap energy, calculated as the difference between the LUMO and HOMO energies, is 4.7255 eV. This bandgap indicates the electronic excitation energy and can be correlated with the molecule's conductivity and optical properties. A larger gap suggests that the compound is less conductive and more chemically stable.

Further descriptors include chemical hardness (η), which is 2.3627 eV, reflecting the resistance to change in the electron distribution of the molecule. Its inverse, softness (S), is 0.4232 eV^{-1}, indicating a moderate ability of the molecule to adapt its electron distribution. The chemical potential (μ) is 3.416 eV, showing the escaping tendency of electrons from equilibrium. The electronegativity (χ), also -3.416 eV, reflects the molecule's ability to attract electrons. Lastly, the electrophilicity index (ω) is 2.4694 eV, quantifying the molecule's ability to accept electrons; a higher value denotes a stronger electrophile. These parameters collectively provide insight into the chemical reactivity, stability, and potential applications of the 4TC compound in areas such as organic electronics or photovoltaics.

Table 4. Calculated Bang gap energy, Hardness (η), Softness (S), Chemical potential (μ), Electronegativity (χ) and Globalphilicity (ω).

Name	HOMO (eV)	LUMO (eV)	Bandgap energy (eV)	η (eV)	S (eV^{-1})	μ (eV)	χ (eV)	ω (eV)
4TC	-5.779	-1.0533	4.7255	2.3627	0.4232	3.416	-3.416	2.4694

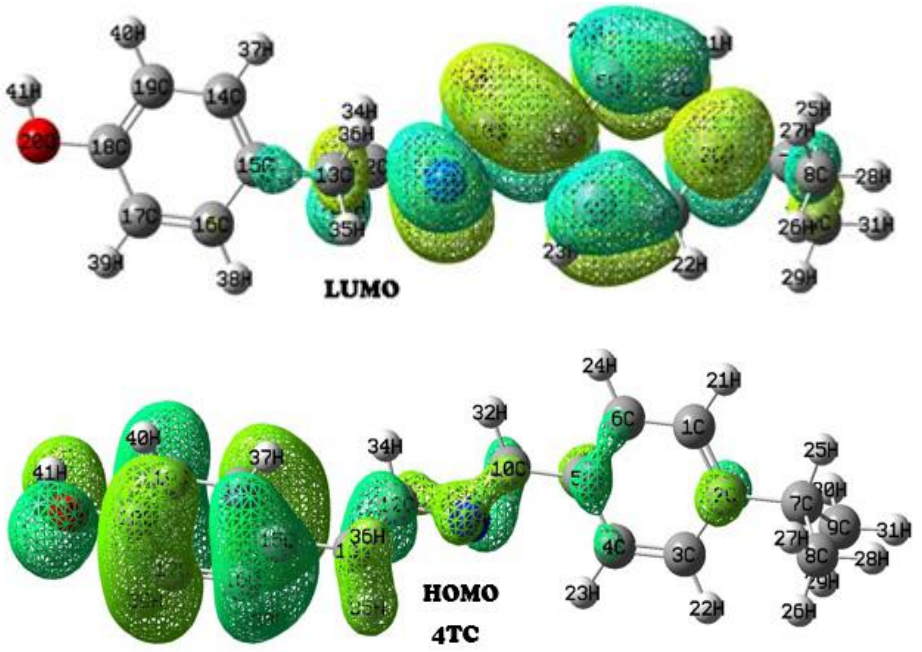

Fig. 5. HOMO-LUMO picture of 4TC.

4.7. *Anticancer activity*

The anticancer activity of the title compound 4TC is analyzed on two human cancer cell lines, MDA MB 231 (human breast cancer cell line) and A549 (human lung cancer cell line); the IC_{50} values of the cancer cell lines are >100 μg/mL and tabulated in Table 5. The MDA MB 231 human breast cancer cell line has a percentage viability of 79.02 μg/mL at the maximum concentration of 100 μg/mL of the title compound. Similarly, the A549 human lung cancer cell line has a percentage viability of 76.16 μg/mL. Accordingly, based on the above experiment, the antitumour activity of 4TC has mild action against two cancer cell lines.

Table 5. Percentage of viability for varying concentration of 4TC for cancer cell lines.

MDA-MB 231		A-549	
Concentration (µg/mL)	Percentage of viability	Concentration (µg/mL)	Percentage of viability
6.25	99.15	6.25	98.57
12.5	97.74	12.5	96.48
25	93.86	25	91.53
50	86.45	50	85.46
100	79.02	100	76.16
IC 50	>100 µg/mL	IC 50	>100 µg/mL

4.8. *Swiss-ADME and Pre-ADME*

Physicochemical properties, druglikeliness and pharmacokinetic properties of the compound 4TC are described by Swiss-ADME (Absorption, Distribution, Metabolism and Excretion of the drug). The physicochemical and drug-likeness properties of the compounds 4TC are given in Table 6. The compound does not violate any of the rules of Lipinski, Ghose, Verber, Egan, and Muegge and shows no violation in PAINS, which gives the information about false positives, i.e., toxic nature in the drug discovery process. In Brenk, the compound 4TC shows 1 alert because of the imine group [34,35]. The synthetic accessibility score (SAS) gives information about the ease of the chemical synthesis of the compounds, which is based on the similarities of the structure of the compound or the fragments in it with existing molecules. The compounds with an SA score less than or equal to 1 are easy to synthesize, and the compounds greater than 10 are difficult to synthesize. The compounds with SA scores between 1 and 10 are at a moderate level. The compound 4TC shows an SA score of 2.37.

Table 6. Physicochemical and Drug likeness properties of 4TC by Swiss-ADME.

Physiochemical properties		Drug likeness properties	
Molecular Formula	$C_{18}H_{21}NO$	Lipinski	Yes
Molecular weight	267.37	Ghose	Yes
No. of heavy atoms	20	Veber	Yes
No. of aromatic heavy atoms	12	Egan	Yes
Fraction Csp3	0.28	Muegge	Yes
No. of rotatable bonds	5	Bioavailability Score	0.55
No. of H-bond acceptors	2	PAINS	0 alerts
No. of H-bond donors	1	Brenk	1 alert (imine group)
Molar refractivity	85.8	Lead likeness	1
-	-	Synthetic Accessibility	2.37

The pharmacokinetic data of the compound 4TC is illustrated by utilizing the web-science tools Swiss-ADME and Pre-ADME and tabulated in Table 7. Passive gastrointestinal (HIA) absorption and blood-brain barrier (BBB) permeation are predicted with the BOILED-EGG (Brain or Intestinal EstimateD Permeation) model illustrated in Fig. 6. The compound 4TC has BBB permeation and a high GI absorption of 96.8, and the compound is a P-gp substrate and has a negative value of skin permeability. The compound

is mutagenic in Ame's test, which demonstrates that the compound can alter the sequence of human DNA. The negative result of carcinogenic mice and rats shows in nature. Based on the log-s scale value of pure water, solubility is described for the compound 4TC. The compound has the highest value, i.e., ≥ 0 (15.80 and 85.90), of pure water solubility, showing that the compound is highly soluble in pure water. The bioavailability value 0.55 denoted that the compounds have no violations against the rule of five (Lipinski rule).

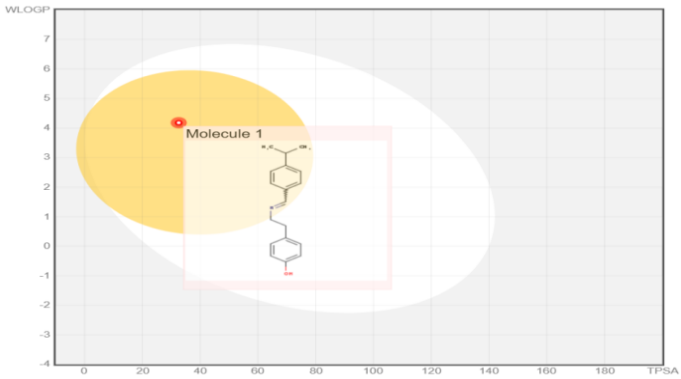

Fig. 6. BOILED EGG diagram of 4TC.

Table 7. Comparison table of pharmacokinetics data of 4TC and 4TN by swiss-ADME and pre-ADME.

Pharmacokinetics	Swiss-ADME	Pre-ADME
GI absorption	High	96.8
BBB permeant	Yes	5.61
Pgp substrate	No	Inhibitor
log Kp (cm/s) Skin permeation	-4.93	-1.66
Ames test	-	mutagen
Carcino_Mouse	-	negative
Carcino_Rat	-	negative

4.9. *In-silico anti-bacterial and anti-fungal activity*

The pass online web science helps to predict the ability of chemical compounds to inhibit the growth of 353 varieties of bacteria in concentrations below 10000 nm [36]. Using the web science, one could select the most promising chemical compound for synthesis and determine the priorities for testing of their antibacterial activity. The activity percentage of various bacteria was analyzed against the compound 4TC, showing a significant level of inhibition, which is shown in Table 8. The compound 4TC shows the highest activity percentage for *Pseudomonas fluorescens,* a rod-shaped and gram-negative bacterium which is detected on the surface of water, solid and plants. In 4TC the next highest activity is absorbed for *bacillus subtilis* a gram positive and human pathogenic bacteria which is present in gut microbiome and soil. The next highest activity percentage for the compound 4TC is given by *Corynebacterium jeikeium, Porphyromonas gingivalis* and *Streptococcus*

mutans bacteria. The antifungal activity of the compounds 4TC is conducted on 38 different types of fungi in concentrations below 5000 nm and is tabulated in Table 8 [38]. The compound 4TC shows higher activity against *Trichophyton mentagrophytes* with 22.35 % and 13.79 % against *Epidermophyton floccosum* and nearly 10 % activity for *Saccharomyces cerevisiae* and *Trichosporon asahii.*

Table 8. Antibacterial and antifungal activity of 4TC.

Bacteria	Activity ≥ 10 %	Fungi	Activity %
Pseudomonas fluorescens	53.24	*Trichophyton mentagrophytes*	22.35
Bacillus subtilis subsp. subtilis str. 168	31.34	*Microsporumcanis*	8.94
Corynebacterium jeikeium	24.81	*Mucor*	-
Porphyromonasgingivalis	22.00	*Saccharomyces cerevisiae*	10.12
Streptococcus mutans	21.11	*Epidermophyton floccosum*	13.79
Staphylococcus simulans	13.76	*Trichosporonasahii*	10.64
Mycobacterium avium	12.63	*Cryptococcus bacillisporus*	8.15
Bacteroides stercoris	12.36	*Aspergillus terreus*	5.52
-	-	*Rhizopus oryzae*	5
-	-	*Pichia guilliermondii*	1.06

5. Conclusion

A novel 74-((E)-2-(4-isopropylbenzylideneamino)ethyl)phenol (4TC) was prepared and characterized by UV and FT-IR spectral studies. The stable conformer of 4TC is deduced by the DFT method and subjected to theoretical FT-IR frequencies calculation. The UV-Vis spectrum of the compound had peak at 303 nm shows the presence of C=N imine group conjugation with aromatic ring and in good agreement with the theoretical value. The first hyperpolarizability of 4TC (β_{tot}) is 50 % greater than that of urea, and hence this molecule can have considerable NLO activity. The MEP surface analysis indicate the electrophilic attacking sites (N_{11} and O_{20}) and the nucleophilic attacking site H_{41}. The anticancer activity was evaluated through a cell viability assay (MTT assay) performed on two cell lines: MDA MB 231 (human breast cancer cell line) and A549 (human lung cancer cell line); the IC_{50} values of the cancer cell lines are >100 µg/mL The MDA MB 231 human breast cancer cell line has a percentage viability of 79.02 µg/mL at the maximum concentration of 100 µg/mL of the title compound. Similarly, the A549 human lung cancer cell line has a percentage viability of 76.16 µg/mL. Accordingly, based on the above experiment, the antitumour activity of 4TC has mild action against two cancer cell lines. In-silico, swiss-ADME and Pre-ADME predictions shows the physiochemical properties, Drug likeness properties and pharmacokinetics of the title compound. The compound 4TC shows the highest activity percentage for *Pseudomonas fluorescens,* a gram-negative bacteria and shows higher antifungal activity against *Trichophyton mentagrophytes* with 22.35 %.

References

1. M. K. Roy, M. S. Alam, M. M. Hossain, R. Hossain, M. Ruknozzaman, and K. Uddin, J. Sci. Res. **17**, 561 (2025). https://doi.org/10.3329/jsr.v17i2.76119
2. N. Ye, Z. Yang, and Y. Liu, Drug Discov. Today **27**, 1411 (2021). https://doi.org/10.1016/j.drudis.2021.12.017
3. M. V. Berridge and A. S. Tan, Arch. Biochem. Biophys. **303**, 474 (1993). https://doi.org/10.1006/abbi.1993.1311
4. D. Ahire, B. Prasad, A. Basit, L. Kruger, S. Sharma,and V. S. Mettu, Pharmacol. Rev. **74**, 771 (2022). https://doi.org/10.1124/pharmrev.121.000449
5. L. Amiranashvili, A. Petrou, N. Nadaraia, V. Poroikov, D. Druzhilovskiy, J. Glamočlija, C. Kamoutsis, P. Pogodin, M. Sokovic, M. Merlani, A. Ciric, and A. Geronikaki, Antibiotics **9**, 224 (2020). https://doi.org/10.3390/antibiotics9050224
6. F. Neese, Coord. Chem. Rev. **253**, 526 (2008). https://doi.org/10.1016/j.ccr.2008.05.014
7. J. B. Nicholas, Top. Catal. **4**, 157 (1997). https://doi.org/10.1023/a:1019179903977
8. F. A. Cotton and X. Feng, J. Am. Chem. Soc. **119**, 7514 (1997). https://doi.org/10.1021/ja9705351
9. D. Gibney, J. N. Boyn, and D. A. Mazziotti, J. Phys. Chem. Lett. **13**, 1382 (2022). https://doi.org/10.1021/acs.jpclett.2c00083
10. M. Rahuman and Habib, Heliyon **6**, ID e04976 (2020). https://doi.org/10.1016/j.heliyon.2020.e04976
11. M. H. Jamróz, Spectrochim Acta A: Mol. Biomol. Spectrosc. **114**, 220 (2013). https://doi.org/10.1016/j.saa.2013.05.096
12. X. J. Yang, R. Glaser, A. Li, and J. X. Zhong, Monthly Notices Royal Astronom. Soc. J. **462**, 1551 (2016). https://doi.org/10.1093/mnras/stw1740
13. Hirota, Minoru, and K. Kitajima, Bull. Chem. Soc. Jpn. **40**, 2197 (1967). https://doi.org/10.1246/bcsj.40.2197
14. R. M. Khan and S. M. Mlungwana, Phytochemistry **50**, 439 (1999). https://doi.org/10.1016/S0031-9422(98)00478-6
15. N. B. Colthup, Introduction to Infrared and Raman Spectroscopy, 3rd Edition (Elsevier, 1990).
16. R. Ramaekers, J. Pajak, M. Rospenk, and G. Maes, Spectrochim. Acta A: Mol. Biomol. Spectrosc. **61**, 1347 (2004). https://doi.org/10.1016/j.saa.2004.10.003
17. M. Xie, A. Fujii, and Y. Matsuda, J. Phys. Chem. A **119**, 5668 (2015). https://doi.org/10.1021/acs.jpca.5b03406
18. H. Tanak, A. A. Ağar, and O. Büyükgüngör, Spectrochim. Acta A Mol. Biomol. Spectrosc. **118**, 672 (2013). https://doi.org/10.1016/j.saa.2013.08.054
19. G. Wojciechowski, M. Ratajczak-Sitarz, A. Katrusiak, W. Schilf, P. Przybylski, and B. Brzezinski, J. Mol. Struc. **650**, 191 (2003). https://doi.org/10.1016/s0022-2860(03)00159-5
20. C. L. Losq, G. D. Cody, and B. O. Mysen, Am. Mineral **100**, 945 (2015). https://doi.org/10.2138/am-2015-5076
21. M. Maj, C. Ahn, B. Błasiak, K. Kwak, H. Han, and M. Cho, J. Phys. Chem. B **120**, 10167 (2016). https://doi.org/10.1021/acs.jpcb.6b04319
22. A. Alphonsa and Therasa, J. Mol. Struc. **1100**, 137 (2015). https://doi.org/10.1016/j.molstruc.2015.07.024
23. S. K. Lanke and N. Sekar, J. Fluoresc. **25**, 1469 (2015). https://doi.org/10.1007/s10895-015-1638-6
24. P. S. Liyanage, R. M. D. Silva, and K. M. N. D. Silva, J. Mol. Struc. **639**, 195 (2003). https://doi.org/10.1016/j.theochem.2003.08.009
25. P. S. Patil and N. Sekar, J. Photochem. Photobiol. A: Chem. **446**, ID 115151 (2023). https://doi.org/10.1016/j.jphotochem.2023.115151
26. P. G. Lacroix, J. A. Delaire, K. Nakatani, G. Iftime, A. C. Razus, and I. Malfant, Chem. Eur. J. **6**, 2599 (2000). https://doi.org/10.1002/1521-3765(20000717)6:14<2599::AID-CHEM2599>3.0.CO;2-G

27. S. Lakshminarayanan, V. Jeyasingh, K. Murugesan, N. Selvapalam, and G. Dass, J. Photochem. Photobiol. **6**, ID 100022 (2021). https://doi.org/10.1016/j.jpap.2021.100022
28. S. Sarala, S. K. Geetha, F. B. Asif, and S. Muthu, Chem. Data Coll. **33**, ID 100699 (2021). https://doi.org/10.1016/j.cdc.2021.100699
29. V. Vidhya, A. Austine, and M. Arivazhagan, Heliyon **5**, ID e02365 (2019). https://doi.org/10.1016/j.heliyon.2019.e02365
30. S. Sudha, M. Karabacak, M. Kurt, M. Cinar, and N. Sundaraganesan, Spectrochim. Acta A: Mol. Biomol. Spectrosc. **84**, 184 (2011). https://doi.org/10.1016/j.saa.2011.09.028
31. R. Parthasarathi, J. Padmanabhan, M. Elango, V. Subramanian, and P. Chattaraj, Chem. Phys. Lett. **394**, 225 (2004). https://doi.org/10.1016/j.cplett.2004.07.002
32. S. Saravanan and V. Balachandran, Spectrochim. Acta A: Mol. Biomol. Spectrosc. **130**, 604 (2014). https://doi.org/10.1016/j.saa.2014.04.058
33. R. Parr, R. Donnelly, M. Levy, and W. Palke, J. Chem. Phys. **68**, 3801 (1978). https://doi.org/10.1063/1.436185
34. M. R. F. Pratama, S. Siswodiharjo, and H. Poerwono, J. Physiol. Pharmacol. **30**, ID 20190251 (2019). https://doi.org/10.1515/jbcpp-2019-0251
35. F. L. Zhao, G. H. Yang, S. Xiang, D. D. Gao, and C. Zeng, J. Biomol. Struct. Dyn. **35**, 427 (2016). https://doi.org/10.1080/07391102.2016.1146165
36. S. L. Dhonnar, R. A. More, V. A. Adole, B. S. Jagdale, N. V. Sadgir, and S. S. Chobe, J. Mol. Struc. **1253**, ID 132216 (2021). https://doi.org/10.1016/j.molstruc.2021.132216
37. U. Singh, P. Singh, A. K. Singh, L. Laxmi, D. Kumar, R. Tilak, S. K. Shrivastava, and R. K. Asthana, Algal Res. **54**, ID 102215 (2021). https://doi.org/10.1016/j.algal.2021.102215
38. D. D. Parab and H. K. Kohli, J. Sci. Res. **17**, 547 (2025). https://doi.org/10.3329/jsr.v17i2.75876